Unveiling Crystalline Order from Glassy Behavior of Charged Rods at Very Low Salt Concentrations

Hanna Anop,[1] Laura Dal Compare,[2] Frédéric Nallet,[1] Achille Giacometti,[2,3] and Eric Grelet[1,*]
[1]Univ. Bordeaux, CNRS, Centre de Recherche Paul-Pascal (CRPP, UMR 5031), 115 Avenue Schweitzer, F-33600 Pessac, France
[2]Dipartimento di Scienze Molecolari e Nanosistemi, Università Ca' Foscari di Venezia Campus Scientifico, Edificio Alfa, via Torino 155,30170 Venezia Mestre, Italy
[3]European Centre for Living Technology (ECLT) Ca' Bottacin, 3911 Dorsoduro Calle Crosera, 30123 Venice, Italy

(Received 20 May 2024; accepted 24 February 2025; published 18 March 2025)

Charged colloids can form ordered structures like Wigner crystals or glasses at very low concentrations due to long-range electrostatic repulsions. Here, we combine small-angle x-ray scattering (SAXS) and optical experiments with simulations to investigate the phase behavior of charged rodlike colloids across a wide range of salt concentrations and packing fractions. At ultralow ionic strength and packing fractions, we reveal both experimentally and numerically a direct transition from a nematic to a crystalline smectic-B phase, previously identified as a glass state. This transition, bypassing the smectic-A intermediate phase, results from minimizing Coulomb repulsion and maximizing entropic gains due to fluctuations in the crystalline structure. This demonstrates how *long-range* electrostatic repulsion significantly alters the phase behavior of rod-shaped particles and highlights its key role in driving the self-organization of anisotropic particles.

DOI: 10.1103/PhysRevLett.134.118101

In 1934 Eugene Wigner suggested the possibility of observing a crystalline state for electrons in a uniform background of positive charges at very low densities and sufficiently low temperatures [1,2]. This occurs because at low densities the potential energy becomes larger than the kinetic one, thus resulting in the possibility of spatial ordering in a crystalline state. While a rigorous proof of Wigner's conjecture has been a quest for many years [3–5], this concept has been extended analogously in soft condensed matter [6,7]. Here, Wigner crystals (glasses) are assigned to any systems able to crystallize (freeze in a kinetically arrested state) at *low packing fraction* and stabilized by *strong long-range electrostatic repulsion* [7–13]. While the formation of ordered states by mutual repulsion between like-charged particles has already been demonstrated [14–18], colloidal Wigner crystals and glasses additionally require an ultralow ionic strength, so that the Debye screening length κ^{-1}, which sets the range of electrostatic repulsions, is many particle diameters, D, and therefore the interaction between particles is nearly Coulombic ($\kappa D \ll 1$) [9–11,19,20].

For rodlike charged particles the counterpart of a Wigner crystal would be the crystalline smectic-B phase, combining lamellar organization normal to the layers and 2D long-range hexagonal order within the layers. The smectic-B phase differs from the liquid-crystalline smectic-A phase, which has liquidlike order within the layers. Because of their shape anisotropy, rodlike particles display more complex phase behavior compared to spherical ones, with the formation of different liquid crystalline phases [21], from orientationally ordered nematic (N) to smectic-A, (SmA), smectic-B (SmB), and columnar (Col) phases as shown experimentally [22–28], theoretically [29–31], and numerically [32–35]. Such a phase behavior is fundamentally driven by excluded volume that has been extended to charged rods by introducing a charge- and ionic-strength-dependent effective diameter accounting for the electrical double layer thickness in case of *screened* electrostatic interaction [21]. In the opposite limit where long-range Coulomb interaction prevails ($\kappa D \ll 1$), much less is known especially considering highly anisotropic particles [36–39]. The complexity increases as two glass transitions associated with the translational and rotational orderings have been observed for colloidal ellipsoids both in 2D [40] and 3D [41]. For rodlike objects, a promising system for observing a Wigner state is highly charged monodisperse filamentous *fd* viruses, which are widely used as a paradigm of slender particles in soft matter physics. At low densities and low ionic strength, Kang and Dhont found experimental evidence [42,43] for a Coulomb-stabilized glass transition, suggesting the Wigner *glass* [44] scenario over the Wigner crystal.

The aim of this Letter is threefold: (1) present conclusive experimental evidence regarding the phase behavior of *fd* virus particles in the regime of very low salt concentrations and low packing fraction; (2) unambiguously show that, under these conditions, the system *crystallizes* from the

*Contact author: eric.grelet@crpp.cnrs.fr

nematic phase, contrary to previous suggestions pointing toward a (Wigner) glass; (3) support these findings with simulations of rodlike charged particles interacting *via* Coulomb potential with tunable screening.

In our experiments, we made use of filamentous bacteriophages, i.e., *fd* viruses, as a paradigmatic example of charged rodlike colloids. These chiral biological objects are monodisperse, long (contour length $L = 880$ nm), thin (diameter $D = 7$ nm), and rather stiff (persistence length $L_p \simeq 3L$) particles. The charge of *fd* virus is not fixed but regulated as the proteins forming the viral capsid possess pH-sensitive amino acids [45]. Such a biological system has often been used for studying the phase behavior of suspensions of charged rods at high ionic strengths ($I_s > 1$ mM). At physiological pH above the isoelectric point pI_E 4.2, *fd* viruses carry a bare negative charge of about $Z_{\text{virus}} \simeq 10000$ [46]. Neglecting charge condensation [28], this leads to counterion concentrations in the millimolar (mM) range for virus suspensions self-organized into liquid crystalline phases (Fig. 1). Therefore, to maintain a *constant* and *low* ionic strength—for which the added salt is not in excess with respect to the counterions—while simultaneously varying the virus concentration, we worked in the semigrand canonical ensemble: *each virus sample at a given concentration* is extensively dialyzed against a CO_2-equilibrated TRIS-HCl solution at pH 6.5 and ionic strength 0.16 mM [47]. This process takes a few weeks to reach equilibrium as shown in Supplemental Material [48] and results in a thick electric double layer for virus particles with a Debye screening length of $\kappa^{-1} = 24$ nm. The mutual electrostatic repulsion between *fd* viruses is therefore long range, with $\kappa D \ll 1$. When faster dialysis is performed combined with the dilution or concentration of the sample, this results in *out-of-equilibrium* samples exhibiting time evolution, close to those reported by Kang and Dhont [42,43].

By increasing the viral rod concentration C_{virus} above the isotropic liquid phase, a chiral nematic (N*) phase first appears as distinguished by its characteristic birefringent fingerprint texture observed through polarizing microscopy [Fig. 1(a)]. The helical periodicity, or cholesteric pitch P, can be measured and falls within the range of approximately 150 to 300 μm, consistent with other studies conducted at higher ionic strengths [54]. Since the cholesteric periodicity far exceeds the other structural length scales in the system, our rod suspension can be approximated as a nematic phase when considering its free energy [24]. Upon a further increase in virus concentration, a change of optical texture occurs, as noticed by Kang and Dhont under similar ionic conditions [42,43]. By employing an optical objective with high numerical aperture (Olympus 100× PlanAPO NA = 1.4), a distinct striped pattern can be discerned, characterized by a periodicity $L_{\text{layer}} \simeq 1$ μm [28], much smaller than the helical pitch P. This layered structure is iridescent and corresponds to a

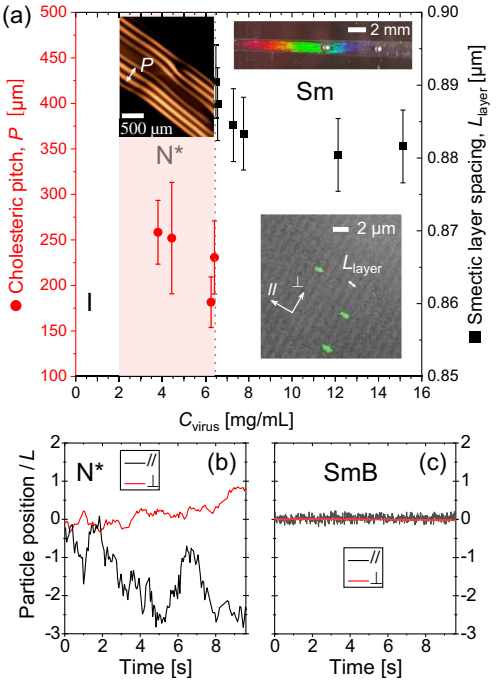

FIG. 1. (a) Optical microscopy experiments revealing the phase behavior of *fd* virus suspensions at low ionic strength ($I_s = 0.16$ mM). Following the isotropic (I) liquid phase, the typical fingerprint texture observed between crossed polarizers (left top inset) characteristic of the chiral nematic (N*) phase can be identified, from which the helical cholesteric periodicity, or pitch P, can be measured (red dots in the light red area). With increasing further virus concentration, a smectic phase forms with a layer spacing $L_{\text{layer}} \simeq 1$ μm measured by differential interference contrast microscopy (bottom right inset). The micrometer-scale periodicity (full black squares) of the lamellar ordering results in Bragg reflections in the visible range making the sample iridescent (top right inset). (b),(c) The dynamics of the system can be probed by single-particle tracking, thanks to a few labeled viral rods as illustrated in the bottom right inset in (a). Anisotropic diffusion is evidenced in the N* phase in contrast to the lamellar phase where the dynamics is nearly frozen with no detectable motion indicating a SmB ordering.

lamellar—or smectic—organization, where viruses with a contour length of $L \simeq L_{\text{layer}}$, stand normal to the layers, as evidenced by the doping of samples with dye-labeled rods [Fig. 1(a)]. Leveraging the presence of such fluorescent viruses, the dynamics of the system has been probed via single-particle tracking, with examples of traces provided for the two ordered phases [Figs. 1(b) and 1(c)]. In the N* phase, a typical Brownian diffusion consistent with nematiclike ordering is observed, characterized by enhanced motion of the rods parallel to their long axis [55]. Conversely, in the Sm state, no significant motion can be detected within the limit of spatial and time resolution of the experimental setup. This nearly frozen dynamics contrasts with the hopping-type diffusion observed in the SmA phase [56], and rather suggests crystalline SmB

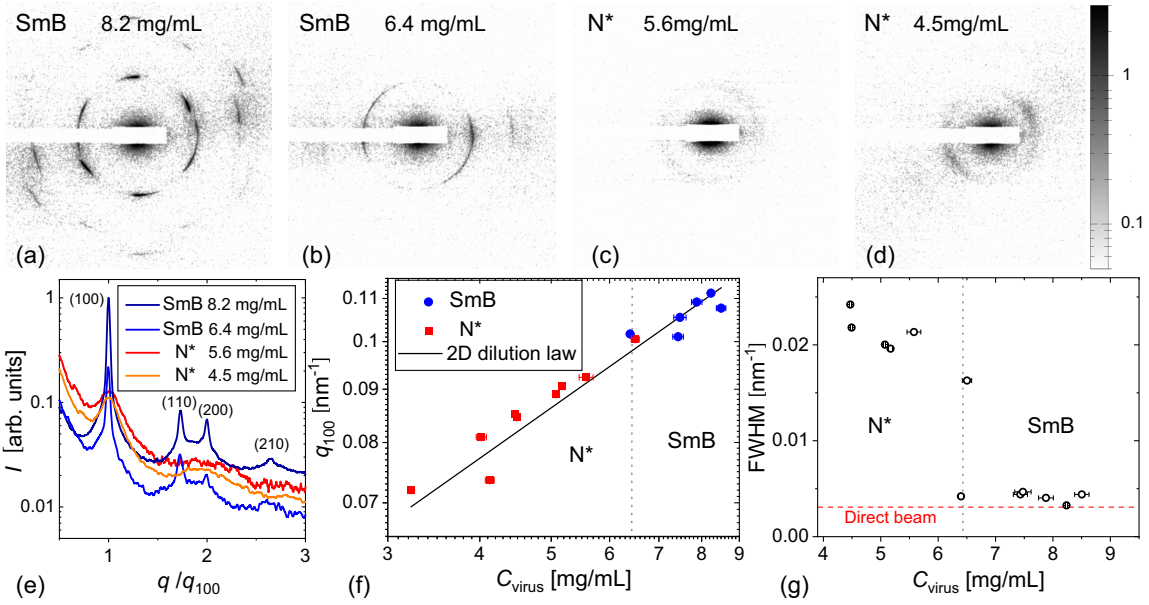

FIG. 2. (a)–(d): X-ray scattering patterns probing the in-plane order normal to the long-rod axis at different virus concentrations (constant ionic strength $I_s = 0.16$ mM), and (e) the corresponding scattered intensities as a function of the normalized scattering wave vector q. The high-order Bragg reflections are characteristic of long-range hexagonal order within the smectic layers, which is the signature of a smectic-B phase for the highest concentrations, i.e., for $C_{\text{virus}} > 6.4$ mg/mL as shown in (e) and (f). (f) The dilution behavior of virus suspensions follows a 2D swelling law ($q_{100} \propto C_{\text{virus}}^{1/2}$), observed across all probed concentrations [58] and also in simulations (see Supplemental Material [48]). In the (chiral) nematic phase, liquidlike ordering is evidenced by broad reflections and a high full width at halfmaximum (FWHM), (g), which is inversely proportional to the translational correlation length. This contrasts with the crystalline ordering observed in SmB, which is only limited by the instrumental resolution provided by the direct x-ray beam (g).

ordering [57]. It is worth noting here that the abrupt change in particle mobility observed by single particle tracking at the N*-SmB transition is compatible with the claim of a particle arrest in the nematic phase associated with a glass state, as previously reported [42,43]. Indeed, Kang and Dhont observations can be interpreted as a slowly evolving state toward the thermodynamically stable SmB phase. This reinterpretation of their findings, which were based on dynamic results therefore lacking structural information, aligns with our own out-of-equilibrium experiments (see Supplemental Material [48]), which consistently exhibit a transition to a crystalline smectic-B phase.

A definite evidence in favor of a crystalline ordering contiguous to the nematic phase at low added salt is provided by structural investigations. Small-angle X-ray scattering (SAXS) was therefore performed using synchrotron facilities (ID02 beamline, ESRF, France). As $C_{\text{virus}} \simeq 10$ mg/mL corresponds to very dilute suspensions with volume fractions of about 1% and thus to large interrod distances, the use of synchrotron radiation with high brilliance and high resolution is essential to underpin the nature of the in-plane order exhibited by the *fd* virus colloidal suspensions. Working with a 16 keV x-ray beam at a sample-to-detector (Frelon camera, ESRF) distance of 5 m, the full range of virus concentrations was studied, as shown in Fig. 2. For the lowest particle packing fractions ($C_{\text{virus}} < 6.4$ mg/mL), the x-ray scattering patterns display broad peaks [Figs. 2(c) and 2(d)] characteristic of liquidlike order [Figs. 2(e) and 2(g)], consistent with the nematic ordering. In the presence of a glass transition, the SAXS patterns would not change significantly, maintaining a liquidlike ordering. However, with a further increase in particle concentration, sharp, resolution-limited reflections appear [Fig. 2(g)] with multiple orders [Figs. 2(a) and 2(b)]. The sequence in reciprocal space relative to the position of the first Bragg peak is $1:\sqrt{3}:\sqrt{4}:\sqrt{7}$ [Fig. 2(e)], associated with (100), (110), (200), and (210) Miller indices characterizing a long-range hexagonal positional order in the plane normal to the rod long axis, as also confirmed by the nearly sixfold symmetry displayed by the SAXS pattern of Fig. 2(a). Combined with the presence of layers as evidenced by optical microscopy [Fig. 1(a)], this demonstrates the existence of the crystalline smectic-B phase, thereby ruling out the presence of a glass state in such low salt conditions. The *direct* N*-to-SmB transition observed here is remarkable in view of the absence of SmA phase that is usually found as an intermediate phase. A 2D dilution law applies both in the N* and SmB range [Fig. 2(f)]. The interrod distance $d_{\text{inter}} = 4\pi/(\sqrt{3}q_{100})$ can be calculated, and when scaled by the particle diameter D, it results in a ratio $d_{\text{inter}}/D \geq 10$, confirming the

low-density regime and thus justifying the term "Wigner crystal" in this context.

Our experimental findings point toward a scenario where strong Coulomb repulsion, high aspect ratio, and excluded volume combine to promote the formation of a SmB phase at low volume fraction similar in spirit to the Wigner crystal predicted for the electron gas [3]. In the colloidal realm, this phase can be considered equivalent to the Wigner body-centered-cubic (BCC) crystals observed for charged spherical colloids in the same regime, while hard spheres crystallize into a face-centered-cubic (FCC) structure [10]. We now show how this scenario can be rationalized through molecular dynamics simulations, extending analogous numerical studies carried out for charged spheres to charged rodlike colloids [16].

Canonical (NVT) simulations were conducted using the LAMMPS suite [59] complemented with in-house codes for the pre- and postprocessing of data. The system consists of $N = 4608$ rods, with the volume V adjusted to attain a desired volume fraction η. Simulations are initialized from a AAA stacking ordered configuration. Each rod of aspect ratio $L/D = 10$ comprises 20 overlapping beads with interrod interactions modeled through Weeks-Chandler-Andersen (WCA) potential for the excluded volume [60–62], and Yukawa potential for the electrostatic interactions [16,63]. While matching both the range of the Debye screening lengths κ^{-1} and the rod surface charge density to experimental values, we tuned the volume fraction from $\eta = 0.01$ to 0.65. Distinct phases were identified using appropriate order parameters and correlation functions [34] (see Supplemental Material [48]). Particularly instrumental in discerning the onset of a crystalline SmB phase are the parallel $g_{\parallel}(r_{\parallel})$ and perpendicular $g_{\perp}(r_{\perp})$ correlation functions. In the nematic phase, $g_{\parallel}(r_{\parallel})$ exhibits a flat structureless behavior, transitioning to the distinctive peaks of smectic ordering with increasing η [Fig. 3(a)]. Likewise, $g_{\perp}(r_{\perp})$ displays numerous peaks [Fig. 3(b)] associated with Miller indices akin to those observed in the SAXS experiments [Fig. 2(e)] for the SmB phase.

The numerical phase diagram in the η–κD plane can now be compared with the corresponding experimental one, as shown in Fig. 4. In the latter, results from different experiments at higher ionic strengths ($\kappa D > 1$) are also reported in addition to those stemming from the present study, with the inset highlighting the low screening, low density behavior. While under strong screening conditions ($\kappa D \gg 1$) the behavior is primarily driven by entropy, i.e., excluded volume, with the usual phase sequence, I-N-SmA-SmB/Col phases, the behavior at low screening conditions ($\kappa D \approx 1$) appears to be significantly different, with progressive shrinking or even disappearance of the isotropic, nematic and smectic-A phases. This leads, in simulations, to solely a crystallike ordering (i.e., either SmB or Col), when κD is reduced below ≈ 1. Remarkably,

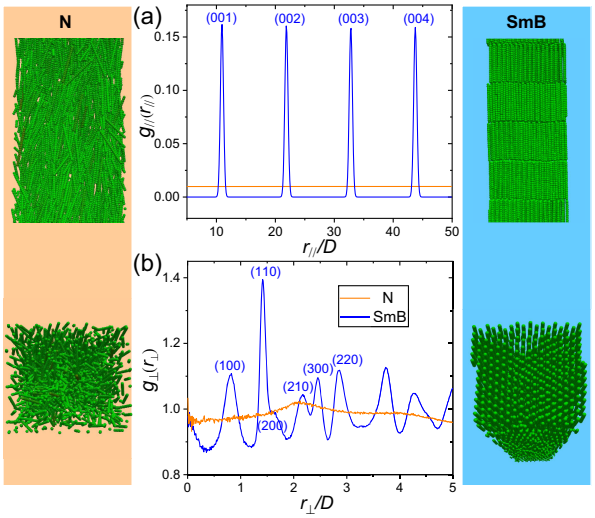

FIG. 3. Parallel (a) and perpendicular (b) pair correlation functions from molecular dynamics simulations at $\kappa D = 3.2$. The volume fraction has been set to $\eta = 0.15$ (orange line) and $\eta = 0.40$ (blue line) corresponding to the nematic and smectic-B phase, respectively.

our simplified model of charged rods qualitatively captures the key features of the experimental phase diagram. Quantitative discrepancies arise primarily from the significant disparity in rod aspect ratio: $L/D = 10$ in simulations (chosen for computational efficiency, see Supplemental Material [48]) vs $L/D \approx 100$ for *fd* virus. This leads to a shift in the location of phase transitions, as predicted by Onsager theory ($\eta_{I-N} \propto D/L$ for slender rods [29]). Incorporating rod flexibility could further improve quantitative agreement [61,64]. Crucially, simulations successfully reproduce the experimental observation of *direct* crystallization into the SmB phase from the nematic state at sufficiently long-range Coulomb repulsion ($\kappa D \approx 2$ to 4), demonstrating the robustness and universality of this phase behavior, independent of specific rod details.

Our results are reminiscent of calculations performed for hard-core, repulsive Yukawa spherical particles, for which the introduction of soft electrostatic interactions promote the formation of a FCC crystal at lower volume fractions as κ^{-1} increases, as well as the onset of a new BCC crystalline phase that is not present in the purely hard-sphere counterpart [16]. Indeed, as shown experimentally [10], the soft interactions in a colloidal Wigner crystal allow for substantial fluctuations of particles within the crystal lattice. Albeit with a shorter lattice spacing than the FCC lattice for the same particle volume fraction η, BCC with only eight nearest neighbors becomes entropically favored compared to the 12 nearest neighbors FCC for η low enough. Similarly, while in the smectic-B phase, the rod fluctuations may occur differently in the longitudinal and transverse directions relative to the layer orientation, both induce an entropic gain compared to the alternate N or SmA

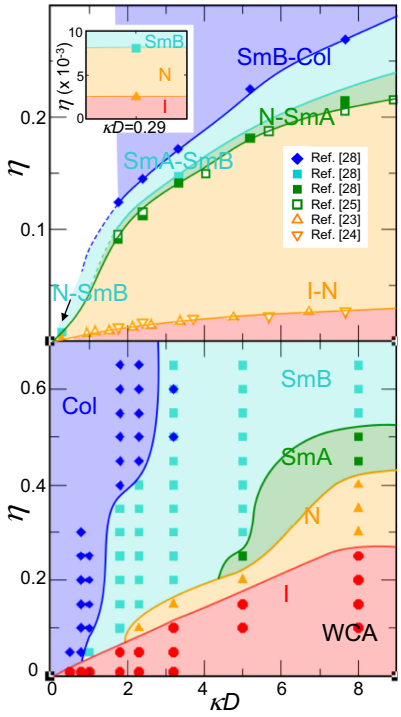

FIG. 4. (top) Experimental phase diagram of the viral rod packing fraction η as a function of κD quantifying the electrostatic screening. The symbols represent the transitions between the different phases, as indicated in the graph. The inset is a magnification of the transitions (I-N and N-SmB) at low ionic strength ($I_s = 0.16$ mM $\Leftrightarrow \kappa D = 0.29$). (bottom) Calculated phase diagram for charged rods exhibiting an aspect ratio of $L/D = 10$. Different colors are associated with the observed thermodynamic phases: isotropic (I, red), nematic (N, orange), smectic-A (SmA, green), smectic-B (SmB, turquoise), and columnar (Col, blue). The WCA column refers to results from hard rods.

structures. When combined with the minimization of Coulomb repulsion due to the low-density conditions, this promotes the SmB stabilization. Additional support to this scenario stems from the average interparticle distance d_{inter} normal to the long-rod axis, which satisfies the condition $d_{\text{inter}} > \kappa^{-1}$ in the Wigner crystal regime, both experimentally and numerically (see Supplemental Material [48]), thus allowing significant fluctuations in the 2D hexagonal lattice.

In summary, we have investigated the experimental phase behavior of highly charged slender rods—filamentous *fd* viruses—under the challenging conditions of very low ionic strengths ($\kappa D \ll 1$) and packing fractions. We have conclusively demonstrated a direct structural phase transition from a nematic to a crystalline smectic-B phase, irrespective of sample preparation and evolution, and proposed a reinterpretation of the former experiments suggesting a Wigner glass transition [42,43]. Our results provide the first conclusive experimental evidence that a system of charged hard rods can form a stable crystal at low concentrations through strong electrostatic repulsions. Strikingly, our findings are well reproduced by extensive numerical calculations of charged rods interacting via excluded volume and screened Coulomb interactions. The onset of a Wigner crystalline smectic-B structure is promoted by the entropic gain due to the large fluctuations around the equilibrium crystal lattice position and represents the rodlike analog of BCC Wigner crystal obtained for charged spherical colloids [10]. Our findings significantly advance our understanding of colloidal liquid crystals in largely unexplored regions of the phase diagram, where the interplay between long-range electrostatic interactions, packing, and entropy leads to intriguing and unexpected phase transitions. This Letter opens pathways for exploring similar phenomena in other anisotropic systems for which the significantly modified phase behavior may be used for the rational design of novel soft self-assembled materials.

Acknowledgments—We thank ID02 staff and the ESRF (Grenoble, France) for the allocated synchrotron beam time (SC-4648). A. Bentaleb is warmly thanked for his help during SAXS experiments. This project has received funding from the European Union Horizon 2020 research and innovation program under the Marie Skłodowska-Curie Grant Agreement No. 641839. A .G. acknowledges financial support by MIUR PRIN-COFIN2022 Grant No. 2022JWAF7Y.

E. G. conceived the study; H. A., E. G., and F. N. conducted the experiments; L .D. C. and A. G. performed the simulations; E. G. wrote the manuscript with contributions from A. G.; all authors edited the manuscript.

[1] E. Wigner, On the interaction of electrons in metals, Phys. Rev. **46**, 1002 (1934).
[2] E. Wigner, Effects of the electron interaction on the energy levels of electrons in metals, Trans. Faraday Soc. **34**, 678 (1938).
[3] G. Giuliani and G. Vignale, *Quantum Theory of the Electron Liquid* (Cambridge University Press, Cambridge, England, 2008).
[4] Y. Zhou, J. Sung, E. Brutschea, I. Esterlis, Y. Wang, G. Scuri, R. J. Gelly, H. Heo, T. Taniguchi, K. Watanabe *et al.*, Bilayer Wigner crystals in a transition metal dichalcogenide heterostructure, Nature (London) **595**, 48 (2021).
[5] T. Smoleński, P. E. Dolgirev, C. Kuhlenkamp, A. Popert, Y. Shimazaki, P. Back, X. Lu, M. Kroner, K. Watanabe, T. Taniguchi, I. Esterlis, E. Demler, and A. Imamoğlu, Signatures of Wigner crystal of electrons in a monolayer semiconductor, Nature (London) **595**, 53 (2021).
[6] P. J. Lu and D. A. Weitz, Colloidal particles: Crystals, glasses, and gels, Annu. Rev. Condens. Matter Phys. **4**, 217 (2013).
[7] E. R. Weeks, Introduction to the colloidal glass transition, ACS Macro Lett. **6**, 27 (2017).

[8] H. M. Lindsay and P. M. Chaikin, Elastic properties of colloidal crystals and glasses, J. Chem. Phys. **76**, 3774 (1982).
[9] M. E. Leunissen, A. van Blaaderen, A. D. Hollingsworth, M. T. Sullivan, and P. M. Chaikin, Electrostatics at the oil–water interface, stability, and order in emulsions and colloids, Proc. Natl. Acad. Sci. U.S.A. **104**, 2585 (2007).
[10] E. R. Russell, F. Spaepen, and D. A. Weitz, Anisotropic elasticity of experimental colloidal Wigner crystals, Phys. Rev. E **91**, 032310 (2015).
[11] J. Everts, N. Boon, and R. van Roij, Density-induced reentrant melting of colloidal Wigner crystals, Phys. Chem. Chem. Phys. **18**, 5211 (2016).
[12] R. Angelini, E. Zaccarelli, F. A. de Melo Marques, M. Sztucki, A. Fluerasu, G. Ruocco, and B. Ruzicka, Glass–glass transition during aging of a colloidal clay, Nat. Commun. **5**, 4049 (2014).
[13] F. Sciortino and P. Tartaglia, Glassy colloidal systems, Adv. Phys. **54**, 471 (2005).
[14] E. B. Sirota, H. D. Ou-Yang, S. K. Sinha, P. M. Chaikin, J. D. Axe, and Y. Fujii, Complete phase diagram of a charged colloidal system: A synchrotron x-ray scattering study, Phys. Rev. Lett. **62**, 1524 (1989).
[15] Y. Monovoukas and A. P. Gast, The experimental phase diagram of charged colloidal suspensions, J. Colloid Interface Sci. **128**, 533 (1989).
[16] A.-P. Hynninen and M. Dijkstra, Phase diagrams of hard-core repulsive Yukawa particles, Phys. Rev. E **68**, 021407 (2003).
[17] A. Yethiraj, Tunable colloids: Control of colloidal phase transitions with tunable interactions, Soft Matter **3**, 1099 (2007).
[18] D. M. Herlach, I. Klassen, P. Wette, and D. Holland-Moritz, Colloids as model systems for metals and alloys: A case study of crystallization, J. Phys. Condens. Matter **22**, 153101 (2010).
[19] E. Zaccarelli, S. Andreev, F. Sciortino, and D. R. Reichman, Numerical investigation of glassy dynamics in low-density systems, Phys. Rev. Lett. **100**, 195701 (2008).
[20] C. L. Klix, C. P. Royall, and H. Tanaka, Structural and dynamical features of multiple metastable glassy states in a colloidal system with competing interactions, Phys. Rev. Lett. **104**, 165702 (2010).
[21] H. N. W. Lekkerkerker, R. Tuinier, and M. Vis, *Colloids and the Depletion Interaction (Second Edition)* (Springer, New York, 2024).
[22] H. Maeda and Y. Maeda, Liquid crystal formation in suspensions of hard rodlike colloidal particles: Direct observation of particle arrangement and self-ordering behavior, Phys. Rev. Lett. **90**, 018303 (2003).
[23] J. Tang and S. Fraden, Isotropic-cholesteric phase transition in colloidal suspensions of filamentous bacteriophage *fd*, Liq. Cryst. **19**, 459 (1995).
[24] K. R. Purdy and S. Fraden, Isotropic-cholesteric phase transition of filamentous virus suspensions as a function of rod length and charge, Phys. Rev. E **70**, 061703 (2004).
[25] K. R. Purdy and S. Fraden, Influence of charge and flexibility on smectic phase formation in filamentous virus suspensions, Phys. Rev. E **76**, 011705 (2007).
[26] E. Grelet, Hexagonal order in crystalline and columnar phases of hard rods, Phys. Rev. Lett. **100**, 168301 (2008).
[27] A. Kuijk, D. V. Byelov, A. V. Petukhov, A. van Blaaderen, and A. Imhof, Phase behavior of colloidal silica rods, Faraday Discuss. **159**, 181 (2012).
[28] E. Grelet, Hard-rod behavior in dense mesophases of semiflexible and rigid charged viruses, Phys. Rev. X **4**, 021053 (2014).
[29] L. Onsager, The effects of shape on the interaction of colloidal particles, Ann. N.Y. Acad. Sci. **51**, 627 (1949).
[30] A. M. Bohle, R. Hołyst, and T. Vilgis, Polydispersity and ordered phases in solutions of rodlike macromolecules, Phys. Rev. Lett. **76**, 1396 (1996).
[31] H. H. Wensink, Columnar versus smectic order in systems of charged colloidal rod, J. Chem. Phys. **126**, 194901 (2007).
[32] A. Stroobants, H. N. W. Lekkerkerker, and T. Odijk, Effect of electrostatic interaction on the liquid crystal phase transition in solutions of rodlike polyelectrolytes, Macromolecules **19**, 2232 (1986).
[33] P. Bolhuis and D. Frenkel, Tracing the phase boundaries of hard spherocylinders, J. Chem. Phys. **106**, 666 (1997).
[34] J. T. Lopes, F. Romano, E. Grelet, L. F. M. Franco, and A. Giacometti, Phase behavior of hard cylinders, J. Chem. Phys. **154**, 104902 (2021).
[35] S. Dussi, M. Chiappini, and M. Dijkstra, On the stability and finite-size effects of a columnar phase in single-component systems of hard-rod-like particles, Mol. Phys. **116**, 2792 (2018).
[36] A. Wierenga, A. P. Philipse, H. N. W. Lekkerkerker, and D. V. Boger, Aqueous dispersions of colloidal boehmite: Structure, dynamics, and yield stress of rod gels, Langmuir **14**, 55 (1998).
[37] C. De Michele, R. Schilling, and F. Sciortino, Dynamics of uniaxial hard ellipsoids, Phys. Rev. Lett. **98**, 265702 (2007).
[38] B. Liu, T. H. Besseling, M. Hermes, A. F. Demirörs, A. Imhof, and A. van Blaaderen, Switching plastic crystals of colloidal rods with electric fields, Nat. Commun. **5**, 3092 (2014).
[39] G. Chu, G. Vasilyev, D. Qu, S. Deng, L. Bai, O. J. Rojas, and E. Zussman, Structural arrest and phase transition in glassy nanocellulose colloids, Langmuir **36**, 979 (2020).
[40] Z. Zheng, F. Wang, and Y. Han, Glass transitions in quasi-two-dimensional suspensions of colloidal ellipsoids, Phys. Rev. Lett. **107**, 065702 (2011).
[41] J. Roller, A. Laganapan, J.-M. Meijer, M. Fuchs, and A. Zumbusch, Observation of liquid glass in suspensions of ellipsoidal colloids, Proc. Natl. Acad. Sci. U.S.A. **118**, e2018072118 (2021).
[42] K. Kang and J. K. G. Dhont, Glass transition in suspensions of charged rods: Structural arrest and texture dynamics, Phys. Rev. Lett. **110**, 015901 (2013).
[43] K. Kang and J. K. Dhont, Structural arrest and texture dynamics in suspensions of charged colloidal rods, Soft Matter **9**, 4401 (2013).
[44] D. Bonn, H. Tanaka, G. Wegdam, H. Kellay, and J. Meunier, Aging of a colloidal "Wigner" glass, Europhys. Lett. **45**, 52 (1999).
[45] P. Passaretti, Y. Sun, T. R. Dafforn, and P. G. Oppenheimer, Determination and characterisation of the surface charge

properties of the bacteriophage m13 to assist bionanoengineering, RSC Adv. **10**, 25385 (2020).
[46] K. Zimmermann, H. Hagedorn, C. C. Heucks, M. Hinrichsen, and H. Ludwig, The ionic properties of the filamentous bacteriophages *Pfl* and *fd*, J. Biol. Chem. **261**, 1653 (1986).
[47] K. Kang, A. Wilk, A. Patkowski, and J. K. G. Dhont, Diffusion of spheres in isotropic and nematic networks of rods: Electrostatic interactions and hydrodynamic screening, J. Chem. Phys. **126**, 214501 (2007).
[48] See Supplemental Material at http://link.aps.org/supplemental/10.1103/PhysRevLett.134.118101 for the details of the virus sample preparation at equilibrium and out of equilibrium, the methods of the molecular dynamics simulations, the definitions of order parameters and anisotropic pair correlation functions, the experimental signature of the SmA phase, the 2D dilution law in simulations, the experimental and numerical dependence of the interrod spacing, the experimental movies displaying the dynamics of individual rods in the N and SmB phases. Supplemental Material also includes Refs. [49–53].
[49] E. Grelet and S. Fraden, What is the origin of chirality in the cholesteric phase of virus suspensions?, Phys. Rev. Lett. **90**, 198302 (2003).
[50] W. G. Hoover, Canonical dynamics: Equilibrium phase-space distributions, Phys. Rev. A **31**, 1695 (1985).
[51] D. Frenkel and B. Smit, *Understanding Molecular Simulation: From Algorithms to Applications* (Elsevier, New York, 2023).
[52] J. Vieillard-Baron, The equation of state of a system of hard spherocylinders, Mol. Phys. **28**, 809 (1974).
[53] A. Stukowski, Visualization and analysis of atomistic simulation data with OVITO-the open visualization tool, Model. Simul. Mater. Sci. Eng. **18** (2010).
[54] E. Grelet and M. M. C. Tortora, Elucidating chirality transfer in liquid crystals of viruses, Nat. Mater. **23**, 1276 (2024).
[55] M. P. Lettinga, E. Barry, and Z. Dogic, Self-diffusion of rodlike viruses in the nematic phase, Europhys. Lett. **71**, 692 (2005).
[56] M. P. Lettinga and E. Grelet, Self-diffusion of rodlike viruses through smectic layers, Phys. Rev. Lett. **99**, 197802 (2007).
[57] L. Alvarez, M. P. Lettinga, and E. Grelet, Fast diffusion of long guest rods in a lamellar phase of short host particles, Phys. Rev. Lett. **118**, 178002 (2017).
[58] E. Grelet and R. Rana, From soft to hard rod behavior in liquid crystalline suspensions of sterically stabilized colloidal filamentous particles, Soft Matter **12**, 4621 (2016).
[59] S. Plimpton, Fast parallel algorithms for short-range molecular dynamics, J. Comput. Phys. **117**, 1 (1995).
[60] D. J. Earl, J. Ilnytskyi, and M. R. Wilson, Computer simulations of soft repulsive spherocylinders, Mol. Phys. **99**, 1719 (2001).
[61] B. De Braaf, M. Oshima Menegon, S. Paquay, and P. Van Der Schoot, Self-organisation of semi-flexible rod-like particles, J. Chem. Phys. **147**, 244901 (2017).
[62] G. Cinacchi, A. Ferrarini, A. Giacometti, and H. B. Kolli, Cholesteric and screw-like nematic phases in systems of helical particles, J. Chem. Phys. **147**, 224903 (2017).
[63] J.-P. Hansen and I. R. McDonald, *Theory of Simple Liquids: With Applications to Soft Matter* (Academic Press, New York, 2013).
[64] Z. Y. Chen, Nematic ordering in semiflexible polymer chains, Macromolecules **26**, 3419 (1993).